Phase Evolution in a Kondo-Correlated System
Yang Ji, *et al.*
Science **290**, 779 (2000);
DOI: 10.1126/science.290.5492.779

opposite polarity and a slightly smaller radius (Fig. 3). The superfluid vortex ring (not shown in the figure) is located between the outer and inner normal-fluid vortex rings, at the position of the forward jet of normal fluid visible in Fig. 2 [a similar structure has been observed by Idowu *et al*. (*27*) in a simpler two-dimensional calculation]. The normal-fluid vortex rings move along with the superfluid vortex ring, even though the largest normal-fluid velocity is always smaller than the velocity of the superfluid vortex ring, V_R. This behavior illustrates that this coupled flow structure is being continuously generated by mutual friction and dissipated rapidly by the normal-fluid viscosity. The superfluid vortex ring shrinks as it moves, providing the energy that is dissipated in the normal fluid.

We observe that the normal-fluid flow structure generated by a superfluid vortex ring moves with the superfluid vortex ring and has the same length scale. The Reynolds number defined using a length scale of $2R$ and a velocity of V_R is $\mathrm{Re} = (\kappa/\nu_n)\{[\log(8R/a) - ½]/2\pi\}$. The term in braces is close to unity for a very large range of R, and the ratio κ/ν_n is of order unity. Thus, the Reynolds number of the normal-fluid part of this flow structure is of order unity.

The qualitative form of the normal-fluid vorticity generated by the superfluid vorticity is important in the interpretation of current turbulence experiments in helium II (*21, 22, 28, 29*). It appears from our calculation that, at least in the parameter regime studied, superfluid vorticity is not able to stir the normal fluid strongly enough to make it turbulent, but rather creates a very dissipative Stokes flow in the normal fluid near the superfluid vortex lines. If we rule out this source of turbulence, then normal-fluid turbulence must then be induced by the boundaries (*21, 28, 29*) or arise from shear flow instabilities (*30*). Only in the case of shear flow instabilities could the mutual friction force with the superfluid directly affect the normal-fluid turbulence.

References and Notes

1. P. G. Saffman, *Vortex Dynamics* (Cambridge Univ. Press, Cambridge, 1992).
2. D. R. Tilley, J. Tilley, *Superfluidity and Superconductivity* (Institute of Physics, Bristol, UK, 1994).
3. R. P. Feynman, *Prog. Low Temp. Phys.* **1**, 17 (1955).
4. R. J. Donnelly, *Quantized Vortices in Helium II* (Cambridge Univ. Press, Cambridge, 1991).
5. R. M. Bowley, P. V. E. McClintock, F. E. Moss, G. G. Nancolas, P. C. E. Stamp, *Philos. Trans. R. Soc. London Ser. A* **307**, 201 (1982).
6. B. Jackson, L. F. McCann, C. S. Adams, *Phys. Rev. A* **60**, 3604 (2000).
7. S. K. Nemirovskii, W. Fiszdon, *Rev. Mod. Phys.* **67**, 37 (1995).
8. B. V. Svistunov, *Phys. Rev. B* **52**, 3647 (1995).
9. W. F. Vinen, *Phys. Rev. B* **61**, 1410 (2000).
10. D. C. Samuels, D. Kivotides, *Phys. Rev. Lett.* **83**, 5306 (1999).
11. G. W. Rayfield, F. Reif, *Phys. Rev. A* **136**, 1194 (1964).
12. C. M. Muirhead, W. F. Vinen. R. J. Donnelly, *Philos. Trans. R. Soc. London Ser. A* **311**, 433 (1984).
13. T. Frisch, Y. Pomeau, S. Rica, *Phys. Rev. Lett.* **69**, 1644 (1992).
14. P. H. Roberts, J. Grant, *J. Phys. A* **4**, 55 (1971).
15. B. Jackson, J. F. McCann, C. S. Adams, *Phys. Rev. Lett.* **80**, 3903 (1998).
16 C. Raman *et al*., *Phys. Rev. Lett.* **83**, 2502 (1999).
17. R. J. Donnelly, in *Quantum Statistical Mechanics in the Natural Sciences,* B. Kursunoglu, S. L. Mintz, S. M. Widmayer, Eds. (Plenum, New York, 1974), pp. 359–403.
18. C. A. Jones, P. H. Roberts, *J. Phys. A* **15**, 2599 (1982).
19. L. Reatto, D. E. Galli, *Int. J. Mod. Phys.* **13**, 607 (1999).
20. G. A. Williams, *J. Low Temp. Phys.* **101**, 421 (1995).
21. M. R. Smith, R. J. Donnelly, N. Goldenfeld, W. F. Vinen, *Phys. Rev. Lett.* **71**, 2583 (1993).
22. S. R. Stalp, L. Skrebek, R. J. Donnelly, *Phys. Rev. Lett.* **82**, 4831 (1999).
23. D. C. Samuels, R. J. Donnelly, *Phys. Rev. Lett.* **65**, 187 (1990).
24. K. W. Schwarz, *Phys. Rev. B* **38**, 2398 (1988).
25. M. Tsubota, S. Maekawa, *Phys. Rev. B* **47**, 12040 (1993).
26. O. C. Idowu, D. Kivotides, C. F. Barenghi, D. C. Samuels, *J. Low Temp. Phys.* **120**, 269 (2000).
27. O. C. Idowu, A. Willis, C. F. Barenghi, D. C. Samuels, *Phys. Rev. B* **62**, 3409 (2000).
28. J. Maurer, P. Tabeling, *Europhys. Lett.* **43**, 29 (1998).
29. M. R. Smith, D. K. Hilton, S. V. VanSciver, *Phys. Fluids* **11**, 751 (1999).
30. D. J. Melotte, C. F. Barenghi, *Phys. Rev. Lett.* **80**, 4181 (1998).

31. Supported by the Leverhulme Trust. We thank W. Dobler for help with the graphics.

3 July 2000; accepted 18 September 2000

Phase Evolution in a Kondo-Correlated System

Yang Ji, M. Heiblum,* D. Sprinzak, D. Mahalu, Hadas Shtrikman

We measured the phase evolution of electrons as they traverse a quantum dot (QD) formed in a two-dimensional electron gas that serves as a localized spin. The traversal phase, determined by embedding the QD in a double path electron interferometer and measuring the quantum interference of the electron wave functions manifested by conductance oscillation as a function of a weak magnetic field, evolved by π radians, a range twice as large as theoretically predicted. As the correlation weakened, a gradual transition to the familiar phase evolution of a QD was observed. The specific phase evolution observed is highly sensitive to the onset of Kondo correlation, possibly serving as an alternative fingerprint of the Kondo effect.

The Kondo effect (*1*), a many-body phenomenon first discovered in metals slightly doped with magnetic impurities, has become one of the paradigms of strongly correlated systems. The effect, a result of an interaction between magnetic impurities with conduction electrons, leads to resonant scattering of Fermi electrons, leading to an abnormal temperature dependence of the conductivity (*2*). It was more recently recognized (*3*, *4*) that the Kondo effect could also take place in a system of a spin-polarized quantum dot (QD) (*5*) strongly coupled to an electron reservoir. Goldhaber-Gordon *et al.* (*6*), and others later, observed clearly such an effect in a QD. Moreover, they were able to control in situ many relevant parameters that affect the Kondo correlation, e.g., the energy level of the localized impurity (the QD) and the coupling strength between the localized impurity and the conduction electrons. Even though the Kondo effect has been studied for some time, one of its most fundamental properties was never experimentally verified: a phase shift of $\pi/2$ experienced by electrons at the Fermi energy scattering of the many-body spin singlet (*7*, *8*), known generally to take place at resonance. The phase evolution in a Kondo-correlated QD was theoretically predicted also to be $\pi/2$ at resonance (*9*). Here, we address this issue experimentally by combining a mesoscopic Kondo-correlated QD with a double path Aharonov-Bohm (AB) interferometer (*10*, *11*). After verifying the coherence of the QD, we proceeded to measure the traversal phase shift of the electrons that pass through the dot.

The QD, serving as a localized spin, is a small, confined puddle of electrons, with two tunnel barriers coupling it to two electron reservoirs. The electrons in the puddle occupy a discrete ladder of energy levels, with level energy ε_d and an average energy separation Δ between non–spin-degenerate levels. A capacitively coupled metallic gate (plunger) is used to tune the energy levels in the dot. Resonant tunneling between the two reservoirs (through the tunnel barrier–dot–tunnel barrier system) occurs and current flows when an energy level in the dot is aligned with the Fermi level in the leads. When one of the electronic levels drops below the Fermi level in the leads, this level becomes occupied and the number of electrons in the dot increases by one. However, due to the small capacitance C of the QD and the discreteness of the electronic charge e, an additional clas-

Braun Center for Submicron Research, Department of Condensed Matter Physics, Weizmann Institute of Science, Rehovot 76100, Israel.

*To whom correspondence should be addressed. E-mail: Heiblum@wisemail.weizmann.ac.il

sical charging energy $U_C = e^2/2C$ is needed in order to add a single electron to the dot. Effectively, the peak spacing can be U_C or $U_C + \Delta$, where typically $U_C \gg \Delta$. At low temperature T ($k_B T \ll U_C$, with k_B as the Boltzmann constant), when the Fermi surface in the leads lays in the gap between energy levels, there is a well-defined number of electrons in the QD and current does not flow. This is the well-known Coulomb Blockade phenomenon, where almost periodic conductance peaks as a function of plunger voltage are separated by almost zero conductance valleys.

While Coulomb Blockade in QDs is a manifestation of the quantization of the electronic charge, the net spin of a QD is also quantized (in units $h/2$, with h as the Planck constant). Using a simplified model, where the strong, many-body interaction among the electrons in a QD is represented only by the charging energy, then generally each energy state is doubly spin degenerate. Hence, the QD is spin polarized (with nonzero net spin) when it contains an odd number of electrons, acting as a magnetic impurity. Furthermore, when the QD is strongly coupled to the leads and the temperature is sufficiently low, a spin singlet can form between the spin-polarized dot and opposite spin electrons in the leads. This correlation leads to an enhancement of the conductance of the valley between two spin-degenerate peaks. The enhancement can be explained by an intuitive, semiclassical approach. Whereas the Coulomb Blockade phenomenon involves resonant tunneling of one electron through one quasi-bound state, the Kondo effect is a second-order quantum mechanical effect involving two electrons simultaneously. There are many possible processes that have to be coherently summed over; here is an example. Having the topmost spin-degenerate energy level singly occupied with a spin-up electron, which can tunnel out to the right lead, allows another electron, with spin down, to simultaneously tunnel in from the left lead. This keeps the number of electrons in the dot constant but leads to a net spin flip in the dot. This process is followed by the return of the spin-up electron from the right lead to the dot accompanied by a simultaneous jump of the spin-down electron to the right lead. The final result is a double spin flip of the dot and net transfer of a spin-down electron from the left lead to the right one, leading to net current transfer (*12*, *13*). In an alternative view, for a dot, modeled as a potential well coupled strongly to two leads, the spin-up electron's wave function leaks from the well to the leads, keeping away the spin-up electrons in the leads due to the Pauli exclusion principle. The spin-down electrons, on the other hand, can get very close to the polarized dot. This can be modeled as an effective attractive potential for spin-down electrons near the dot, leading to the formation of a lower energy spin singlet (Fig. 1A). Due to this attractive potential, which turns out to be most effective for electrons at the Fermi energy, the impinging rate of spin-down electrons on the dot increases, leading to an increased current. The effective transport density of states develops a sharp peak at the Fermi energy (Fig. 1A), with a width reflecting the binding energy of the spin singlet. This small binding energy is customarily described by a Kondo temperature, T_K (about 1 K in our QDs). The Kondo-enhanced valley conductance due to such correlation can be easily quenched by increasing the temperature, applying a finite dc voltage bias across the QD, or diminishing the coupling between the QD and the leads.

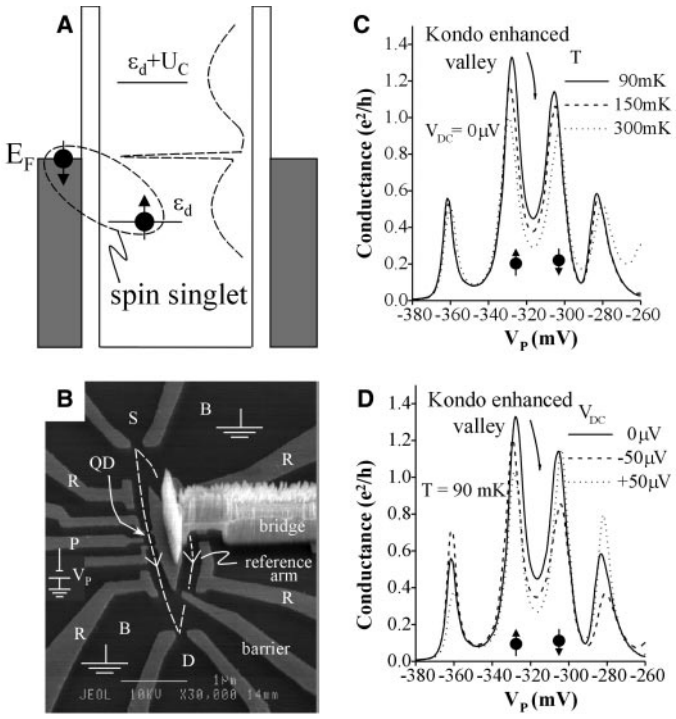

Fig. 1. Kondo-correlated spin singlet, sample description, and characterization of a Kondo pair. (**A**) Energy diagram of a quantum dot with Kondo correlation. The two spin-degenerate energy levels, ε_d and $\varepsilon_d + U_C$, are strongly coupled to the leads. At low temperature, a spin singlet is formed between the localized electron in the QD and an opposite spin electron in the leads, thus leading to a strong resonance in the transport density of states (dashed line) centered at the Fermi level in the leads. (**B**) A top-view picture with a scanning electron microscope of the electronic double path interferometer. The device is defined by negatively biased metallic gates (light gray areas) deposited on the surface of a GaAs-AlGaAs heterostructure with high mobility electrons 55 nm below the surface (density $n = 3 \times 10^{11}$ cm^{-2}, mobility $\mu = 5 \times 10^5$ cm^2 V^{-1} s^{-1}, measured at 1.5 K). Three different regimes can be identified: source (S), drain (D), and base (B). The source and drain openings support only one transverse mode, producing a planar electronic wavefront in the far field. The base regions collect back-scattered electrons to ensure that only the two forward-propagating paths (broken white lines) reach the collector and interfere. A metallic air bridge, formed by special lithographic techniques, is used to deplete the island between the two paths. A quantum dot (area 180 nm by 200 nm) is placed in the left arm, with both of its point contacts and the plunger gate (P) individually controlled. Reflectors (R), confining the two paths, are used to deflect the electrons toward the drain. A barrier gate is used to cut off the reference (right) arm in order to allow tuning of the bare QD to the Kondo regime. Bar, 1 μm. (**C**) The effect of increasing temperature on the conductance with $V_{dc} = 0$ μV across the QD. As the temperature increases, the Kondo enhancement of the central valley becomes smaller. (**D**) The effect of dc bias across the QD on the conductance at $T = 90$ mK. The central valley conductance decreases with increasing dc bias.

Conductance measurements in QDs have already demonstrated the Kondo effect (*6*); however, the issue of coherence and phase evolution in such systems remained open. We used a double path electron interferometer with a QD tuned to the Kondo correlated regime embedded in one of its paths (*11*) (Fig. 1B). In such system, smaller in overall dimensions than the phase breaking length, the current collected in the drain depends both on the magnitude, t_{QD}, and phase, φ_{QD}, of the transmission coefficient of the QD. Because the four base regions collect most of the backscattered electrons, the net transmission amplitude of the electrons going from source (S) to drain (D), t_{SD}, is a coherent sum of the transmission amplitudes of only two direct paths (dashed lines in Fig. 1B). A two-terminal interferometer is not able to measure directly the accumulated phase in one path (*11*) because the reflected paths cannot escape from the interferometer, hence leading to a large number of paths contributing to the interference. With t_{ref}, φ_{ref}, belonging to the reference arm, $t_{SD} = t_{ref} + t_{QD}$ (assuming $t_{left} = t_{QD}$), the collected current in a coherent system is $I_{SD} \propto |t_{SD}|^2 = |t_{ref}|^2 + |t_{QD}|^2 + 2|t_{ref}||t_{QD}|\cos(\varphi_{ref} - \varphi_{QD})$. Introducing a magnetic flux, Φ, in the area encompassed by the two paths, changes the relative

phase of the reference arm via the AB effect (*10*), $\varphi_{ref} \rightarrow \varphi_{ref} + 2\pi\Phi/\Phi_0$, with $\Phi_0 = h/e$ as the flux quantum. This leads to an oscillating periodic component in the current as a function of magnetic field $\propto \cos(\varphi_{ref} - \varphi_{QD} + 2\pi\Phi/\Phi_0)$. The phase evolution in the QD can be directly deduced from the phase of the current oscillation in the drain. Such experiments have already been carried out with QDs in the Coulomb Blockade regime (*11*). There, the measured phase of the QD was found to climb by π as each resonance was swept through the Fermi level in the leads, as theoretically expected. In the valley between the peaks, however, the phase experienced an unexpected abrupt $-\pi$ phase lapse in all valleys, a phenomenon not yet understood.

The double path interferometer is similar to that used in (*11*) (Fig. 1B). It is fabricated in a two-dimensional electron gas (2DEG), embedded in a GaAs-AlGaAs heterostructure, with submicrometer metallic gates deposited on the surface. The QD is made smaller than usual (180 nm by 200 nm) to allow large energy-level spacing, hence allowing strong coupling of the dot to the leads without overlapping of energy levels. There are a few tens of electrons in the dot with an average level spacing $\Delta \cong 0.5$ meV and a charging energy $U_C \cong 1.5$ meV. Another barrier gate was added to shut off the reference arm and allow measuring the conductance of the QD. Measurements were done in a dilution refrigerator with base temperature $T < 50$ mK and an electron temperature $T_{electron} \sim 90$ mK. Current collected in the drain was measured with standard lock-in techniques, with an excitation voltage 10 μV at 7 Hz, applied between the source and the nearby base contacts. Four different samples, fabricated with different size QDs and in different 2DEG systems, were measured. All produced qualitatively similar results.

A Kondo-enhanced valley, confined between a pair of conductance peaks, is usually identified by its higher conductance. It can be quenched by an increased temperature, by an applied finite dc bias across the QD, or by a reduction in the dot's coupling to the leads (*6*). First, an identification of the Kondo pair was performed by measuring the conductance of the QD itself by pinching off the reference arm with the barrier gate. Four conductance peaks as a function of plunger gate voltage are seen in Fig. 1, C and D. At the lowest temperature and zero dc bias, the two center conductance peaks border a relatively high valley. As the temperature was increased (from 90 to 300 mK, Fig. 1C) or the dc bias was raised (0 to ± 50 μV, Fig. 1D), the central valley conductance decreased, the peak heights decreased, and the peak spacing increased—all characteristic of a Kondo-correlated pair (*6*). The conductance of the two outer valleys and peaks remained almost unchanged, consistent with a Coulomb Blockaded transport (*5*).

Having identified the Kondo pair, we removed the barrier gate voltage and formed the source and drain point contacts, thus allowing two paths interference. The drain current as a function of the plunger gate voltage (Fig. 2A) resembles the conductance of the bare QD (Fig. 1C), but the peaks are shifted by some 80 mV in plunger gate voltage, their shape is distorted, and a large background appears. The obvious reason for the shift is the electrostatic influence of the barrier gate and the two point contacts forming the source and drain entries. Shape distortion can be accounted for by the interference of the electron waves arriving from both of the interferometer arms. To perform interference, we induced a controlled phase difference between the two direct paths from S to D by applying a perpendicular magnetic field via the AB effect. The oscillations observed in the drain current (shown, for example, in five different points in Fig. 2, A and B) with period 3.5 mT immediately suggest coherency of transport in the QD, in and out of resonances. Moreover, the high visibility (5 to 25%), suggests that transport through the dot is highly coherent (*10*, *11*). Assuming that the transmission of the reference arm remains unaffected by the plunger gate voltage, each trace of current oscillation (like in Fig. 2B) provides two data points: an average visibility, leading to the magnitude of the transmission amplitude of the QD, and a phase of the oscillation being the phase of the complex transmission amplitude. The visibility and the phase as a function of plunger gate voltage are shown in Fig. 2C. The visibility mimics the conductance of the QD shown in Fig. 1C quite well, suggesting that the coherent transmission and the total transmission are qualitatively similar in the entire energy range. While phase lapses, similar to those observed in (*11*), are observed between non–spin-degenerate levels (near $V_P = -280$ mV, -210 mV), the phase in and between the spin-degenerate levels evolves continuously and monotonously, with no sign of phase lapse. The phase climbs through the spin-up peak and saturates at π in the valley; thereafter, it continues to climb by about $\pi/2$ through the spin-down peak. In other samples not shown here, we find the climb through the spin-down peak to be also close to π. We believe that the total phase change across a Kondo pair varies from one sample to another because of overlapping of peaks that depend on their width and spacing. Hence, the phase seems to evolve by π through the first peak and into the Kondo valley, saturates there (*9*), and continues to climb to 2π across the second spin-degenerate peak. This is in contradiction to the prediction of Gerland *et al.* (*9*), who predicted a saturation of the phase between peaks at $\pi/2$ and a total π phase change across the two spin-degenerate peaks. It is worth noting that in our device, due to the relatively high temperatures of the electrons, we could not reach the full $2e^2/h$ conduction enhancement in the valley (*9*, *13*, *14*). Still, phase behavior is markedly distinct and different from that in the Coulomb Blockade regime.

The Coulomb Blockade regime can easily

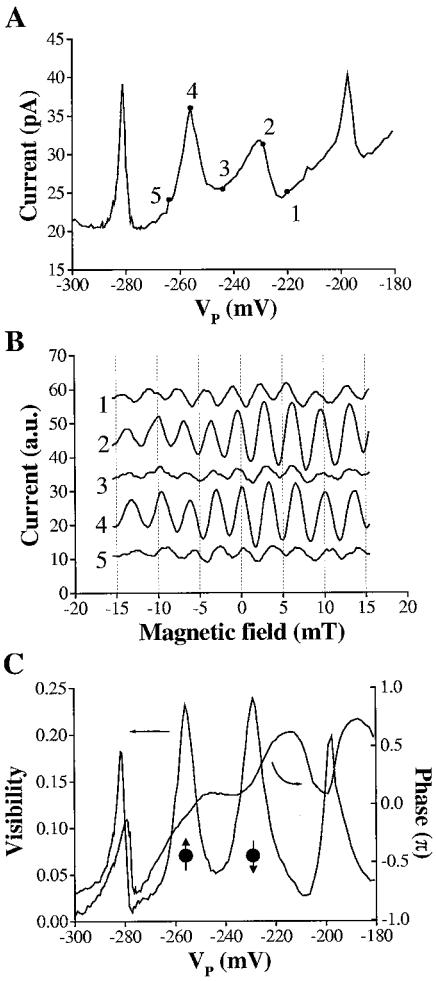

Fig. 2. Complex transmission coefficient of the quantum dot in the Kondo regime measured via the AB effect. (**A**) Collector current as a function of plunger gate voltage at zero magnetic field. This current is very sensitive to magnetic field due to the AB effect, as shown in (**B**), with a series of interference patterns in the current collected by the drain [measured at specific points given in (A) and shifted vertically for clarity]. Trace 3, measured at the center of the conductance valley between the Kondo pair, verifies coherency of electron transport in the Kondo valley. (**C**) Qualitative behavior of the magnitude (shown by the visibility of AB oscillations) and absolute value of the phase of the transmission coefficient of the QD, both obtained from the AB oscillations. The phase evolves continuously through the Kondo pair, whereas there is a phase lapse of $-\pi$ between the other consecutive peaks. Arrows point to the vertical axis to which each curve relates.

be approached by reducing the coupling strength of the QD to the leads. As the coupling strength gradually weakens (Fig. 3, A through D), the phase behavior evolves. From a monotonic increase across the two spin-degenerate peaks with a plateau in the valley for strong coupling, to a behavior with a small phase lapse replacing the plateau in the valley, and eventually a full $-\pi$ phase lapse for the weakest coupling, which is distinctive at Coulomb Blockade transport. As suggested before, the narrowing of the peaks and their reduced overlap allowed greater span of the phase change, namely, a full accumulation of π across each peak. The smooth phase evolution (rather than the phase lapse) in a Kondo valley cannot be interpreted as a simple by-product of the enhanced valley conductance, as can be inferred by observing the results of Figs. 2C, 3A, and 3B.

Increasing the temperature to an order of T_K or applying a bias across the QD to an order of $k_B T_K$ destroys the Kondo correlation (Fig. 1). However, as the electron temperature increases, the visibility tends to decrease because of the shorter dephasing length and phase averaging of the electrons in the interferometer (Fig. 1C). As the temperature increases the phase evolution changes from a smooth and monotonic increase at low temperatures to a phase lapse in the valley. This phase lapse reaches a full $-\pi$ at a temperature of about 1 K (Fig. 4B). Similarly, the application of a small dc bias across the QD at the lowest temperature leads to a similar change in the phase evolution, namely, moving from a smooth increase at $V_{dc} = 0$ μV to a phase lapse at $V_{dc} = 100$ μV (Fig. 4D). In both cases, Kondo correlation ceases to exist at $T \sim T_K \sim 1$ K and $eV_{dc} \sim k_B T_K \sim 100$ μeV.

The results presented here suggest a sensitive, previously unknown fingerprint of Kondo correlation in a QD with spin-degenerate levels. The total accumulated phase as the two spin-degenerate levels cross the Fermi energy in the leads is nearly 2π with a phase shift π in the Kondo valley. Aside from

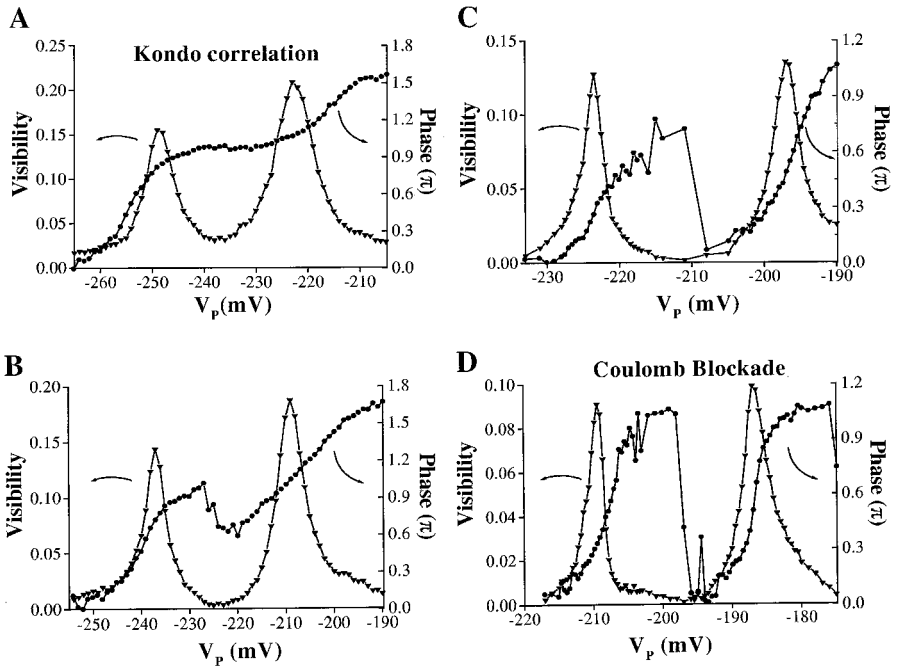

Fig. 3. Phase lapse is formed as the coupling between the quantum dot and the leads is gradually reduced. When the coupling to the leads is strong (**A**), the phase evolution is continuous, with a π plateau in the valley and the total phase change through the spin-degenerate pair of about 1.5π. As the coupling gets weaker [from (A) to (**D**)] and the QD enters the Coulomb Blockade regime, the familiar phase lapse (*11*) is recovered and a full phase evolution of π across each peak emerges. The peak position shifts due to the influence of the voltage applied to the gates that form the two point contacts of the QD. (●), phase; (▼), visibility.

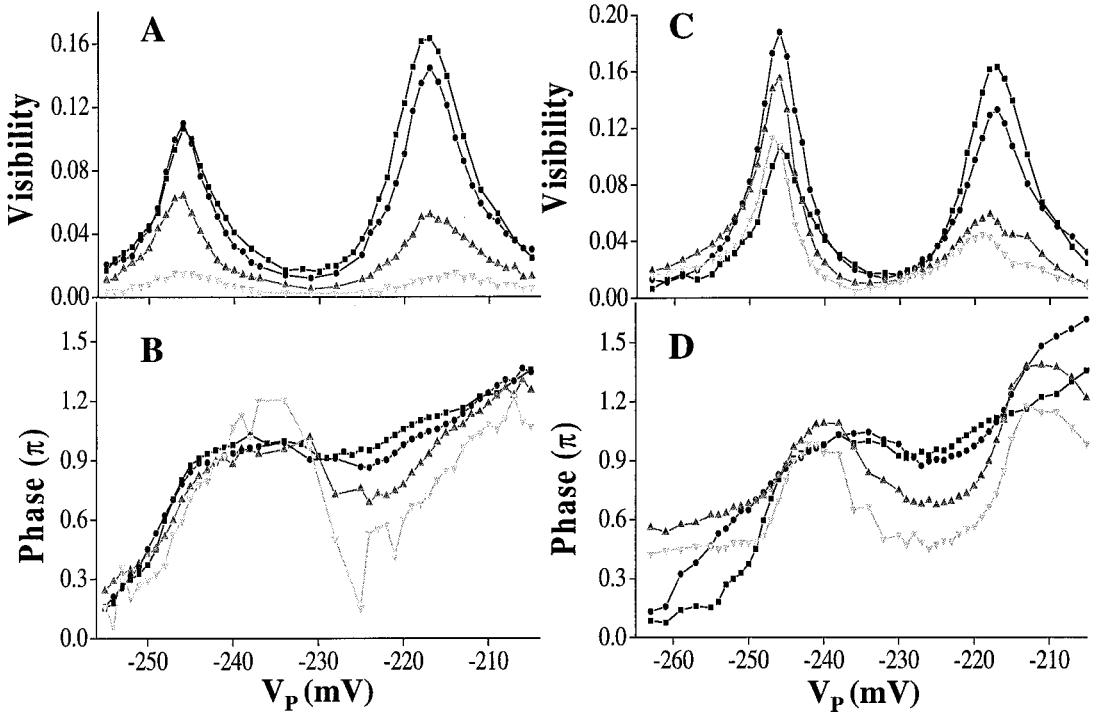

Fig. 4. The effect of temperature and applied dc bias on the phase evolution. (**A**) Qualitative behavior of the magnitude, and (**B**) phase evolution of the transmission coefficient as a function of plunger gate voltage, measured with increasing temperature. V_{dc} in (A) and (B) is 0 μV. Symbols in (A) and (B) are as follows: (■), 90 mK; (●), 150 mK; (▲), 300 mK; (▼), 1000 mK. (**C**) Qualitative behavior of the magnitude and (**D**) phase evolution of the transmission coefficient as a function of plunger gate voltage, measured at 90 mK with increasing dc bias between source and base. (■), 0 μV; (●), −40 μV; (▲), −80 μV; (▼), −100 μV. In both cases, the monotonous phase evolution disappears at some point, and a phase lapse is formed in the valley between the Kondo pair, as the QD approaches the Coulomb Blockade regime.

the saturated behavior of the phase in the valley, our results do not agree with the recent prediction by Gerland *et al.* (*9*), who calculated the saturation of the phase to be at $\pi/2$. Although the conductance usually serves as a qualitative and approximate mark to the onset of the Kondo correlation, the phase evolution has a distinctively different and pronounced behavior in the Kondo regime. This behavior abruptly changes as the Kondo correlation weakens, evolving into the known Coulomb Blockade regime. The reasons for the deviation of the measured phase from the fundamental predictions are presently not clear. We believe that a complete insight into the Kondo-correlated regime can only be achieved after full understanding of the Coulomb Blockade regime.

References and Notes

1. J. Kondo, in *Solid State Physics*, H. Ehrenreicht, F. Seitz, D. Turnbull, Eds. (Academic Press, New York, 1969), vol. 23, pp. 183–281.
2. P. W. Anderson, *Phys. Rev.* **124**, 41 (1961).
3. L. I. Glazman, M. E. Raikh, *JETP Lett.* **47**, 452 (1988).
4. T. K. Ng, P. A. Lee, *Phys. Rev. Lett.* **61**, 1768 (1988).
5. U. Meirav, E. B. Foxman, *Semicond. Sci. Technol.* **10**, 255 (1995).
6. D. Goldhaber-Gordon *et al.*, *Nature* **391**, 156 (1998).
7. D. C. Langreth, *Phys. Rev.* **150**, 516 (1966).
8. P. A. Nozieres, *J. Low Temp. Phys.* **17**, 31 (1974).
9. U. Gerland, J. von Delft, T. A. Costi, Y. Oreg, *Phys. Rev. Lett.* **84**, 3710 (2000).
10. A. Yacoby, M. Heiblum, D. Mahalu, H. Shtrikman, *Phys. Rev. Lett.* **74**, 4047 (1995).
11. R. Schuster *et al.*, *Nature* **385**, 417 (1997).
12. Y. Meir, N. S. Wingreen, P. A. Lee, *Phys. Rev. Lett.* **70**, 2601 (1993).
13. N. S. Wingreen, Y. Meir, *Phys. Rev. B* **49**, 11040 (1994).
14. J. Schmid, J. Weis, K. Eberl, K. von Klitzing, *Phys. Rev. Lett.* **84**, 5824 (2000).

15. We thank D. Goldhaber-Gordon and E. Buks for valuable suggestions on the fabrication process and measurement techniques. We also thank J. von Delft and Y. Oreg for helpful discussions before publication. Supported in part by the MINERVA foundation.

21 July 2000; accepted 20 September 2000

Moissanite: A Window for High-Pressure Experiments

Ji-an Xu and Ho-kwang Mao

We achieved a pressure of 52.1 gigapascals with moissanite anvils, which have optical, thermal, electric, magnetic, and x-ray properties that rival those of diamond. The mode-softening of D_2O toward the pressure-induced hydrogen bond symmetrization and the Raman shifts of diamond under hydrostatic and nonhydrostatic compressions were studied with moissanite anvils in the spectral regions normally obscured by diamond anvils. Moissanite anvil cells allow maximum sample volumes 1000 times larger than those allowed by diamond anvil cells and may enable the next level of advancement in high-pressure experiments.

Sustained breakthroughs in ultrahigh-pressure technology over the past 25 years have had impacts in areas ranging from fundamental physics and chemistry (*1*, *2*) to earth, planetary (*3*), and materials research (*4*). Pressures achievable with the Mao-Bell–type diamond anvil cell (DAC) exceeded the 50-GPa (half-megabar) barrier in 1975 (*5*) and subsequently increased to hundreds of GPa (*6–9*). The DAC thus became the only research tool for static pressure experiments above 30 GPa. The infrared, visible, x-ray transparency, and other favorable properties of diamond provide a window for laser (*10*), x-ray (*11*, *12*), electric (*13*), and magnetic (*14*) microprobes in situ at high pressures. The use of diamonds, however, also imposes limitations. The characteristic infrared, Raman, and Brillouin peaks of diamond interfere with measurements of sample peaks in similar spectral regions. Diamond shows surface oxidation above 900 K and burns above 1120 K in air and must be kept in a reducing atmosphere for experiments at high pressure and temperature (*P-T*) with external heating (*15*). The most severe constraint is that perfect diamonds have limited availability and very high cost, restricting high-pressure samples to microscopic volumes (10^{-10} to 10^{-13} liters).

Previous experiments in the search for superhard gem anvils to use as replacements or complements for diamond have only reached pressures of a maximum of 16.7 GPa with cubic zirconia (*16*) and 25.8 GPa with sapphire (*17*). With a hardness (Knoop scale) of 3000, synthetic moissanite (hexagonal silicon carbide) is harder than sapphire (2000) and cubic zirconia (1370) but softer than diamond (5700 to 10,400). Large, gem-quality, single-crystal moissanite has recently become available (*18*). We carried out experiments using moissanite anvils with the *c* crystallographic direction parallel to the compression axis. The fluorescence spectra of ruby grains compressed without a pressure medium were measured through the moissanite window for pressure calibration (Fig. 1). The moissanite anvils readily achieved 52.1 GPa.

Complementary to diamond, moissanite provides a clear window between 0.4 and 5.5 μm for optical spectroscopy. For instance, moissanite has sharp Raman spectral peaks at 149.6, 766.9, 788.4, and 964.7 cm^{-1} that do not overlap with the first-order Raman peak of diamond at $\nu_0 = 1333$ cm^{-1} or with the broad multiphonon second-order Raman band of diamond in the region from 2300 to 2700 cm^{-1}. High-pressure phase transitions and symmetrization of hydrogen bonds in H_2O and D_2O ices have been characterized by Raman mode-softening (*19–21*). With moissanite anvils, we observed the evolution and splitting of E_g and B_{1g} peaks of D_2O ices in the spectral region from 2300 to 2700 cm^{-1} without the background interference of diamond anvils (Fig. 2).

A fundamental problem for understanding the bonding nature of superhard materials is the effect of hydrostatic and nonhydrostatic stresses on the first-order Raman peak of diamond itself (*22–24*). Separation of the Raman peaks of the diamond samples and the DAC is difficult, particularly at pressures below 10 GPa, when the total shift is less than the bandwidth of the peaks. Isotopic ^{13}C-

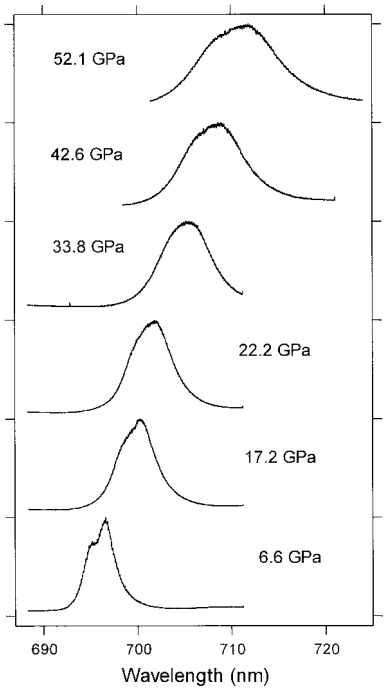

Fig. 1. Ruby fluorescence spectra observed in a MAC up to 52.1 GPa. The experiments were conducted with a moissanite anvil with a 300-μm-diameter flat culet opposing a second anvil with a 300-μm 10° beveled culet with a 100-μm central flat culet.

Center for High Pressure Research and Geophysical Laboratory, Carnegie Institution of Washington, 5251 Broad Branch Road, NW, Washington, DC 20015, USA.